Raman scattering, electronic, and ferroelectric properties of Nd modified $Bi_4Ti_3O_{12}$ nanotube arrays

Di Zhou,[1] Haoshuang Gu,[1,a)] Yongming Hu,[1,2] Zheli Qian,[1] Zhenglong Hu,[1] Kun Yang,[1] Yanan Zou,[1] Zhao Wang,[1] Yu Wang,[2,a)] Jianguo Guan,[3,a)] and Wanping Chen[4]
[1]*State Key Laboratory of Ferro- and Piezoelectric Materials and Device of Hubei Province, Faculty of Physics and Electronic technology, Hubei University, Wuhan 430062, People's Republic of China*
[2]*Materials Research Center and Department of Applied Physics, The Hong Kong Polytechnic University, Kowloon, Hong Kong, People's Republic of China*
[3]*State key Laboratory of Advanced Technology for Materials Synthesis and Processing, Wuhan University of Technology, Wuhan 430070, People's Republic of China*
[4]*Department of Physics and Key Laboratory of Acoustic and Photonic Materials and Devices of Ministry of Education, Wuhan University, Wuhan 430072, People's Republic of China*

(Received 21 June 2009; accepted 24 March 2010; published online 6 May 2010)

Neodymium-modified bismuth titanate, $Bi_{4-x}Nd_xTi_3O_{12}$ (BNdT), nanotube arrays were fabricated by sol-gel method utilizing experimentally prepared porous anodic aluminum oxide (AAO) templates with pore diameters of about 200 nm and 100 nm, respectively. The as-prepared nanotube arrays exhibit orthorhombic perovskite polycrystalline structure of BNdT, which have outer diameters of about 200 and 100 nm, corresponding to the pores diameters of the AAO templates employed, and with wall thicknesses of about 9.7 nm and 12 nm, respectively. The phonon vibration modes corresponding to the Bi atoms in the Bi_2O_2 layers weaken and broaden with increasing Nd content. The changes of Raman internal modes originated from the vibrations of atoms inside the TiO_6 octahedral indicate the increase in octahedron tilting and structural distortion. The leakage current and polarization-electric field response curves of BNdT nanotube arrays were measured, and the hysteresis loop illustrates a good ferroelectric property of as-prepared BNdT nanotube array at room temperature. The dielectric constant and dissipation factor were measured in the frequency region from 1 kHz to 1 MHz indicating polarization relaxation phenomenon. © *2010 American Institute of Physics*. [doi:10.1063/1.3407563]

I. INTRODUCTION

One-dimensional (1D) ferroelectric nanomaterials, such as nanotubes or nanowires are currently attracting great interests due to their potential applications in electrical, thermal transport, and mechanical devices,[1–3] which can provide a good system to study the dependence of properties on dimensionality and size reduction.[4–7] In the last several years, long ferroelectric nanowires/tubes with diameters of 5–70 nm and well defined structures have been fabricated through different methods.[8–13] Among various synthesis methods, sol-gel method has become a popular route for preparing inorganic materials because of its advantages over many other conventional synthetic procedures, such as high purity, homogeneous multicomponent, and easy chemical doping. It is well established that anodic aluminum oxide (AAO) film can provide an ordered porous structure with channel diameters ranging from 10–200 nm, and pore lengths from 1 to over 100 μm, which become an ideal template for the fabrication of 1D nanoarrays.[14] Many 1D nanostructrues have been synthesized using sol-gel AAO template method. For instance, $Pb(Zr,Ti)O_3$ and $Ba_{0.6}Sr_{0.4}TiO_3$ nanotube arrays with outer diameters of 50 nm and 200 nm, respectively, were fabricated.[15,16] $Bi_{3.25}La_{0.75}Ti_3O_{12}$ nanotubes were also prepared by AAO template-wetting process in precursor solutions.[3]

Bismuth titanate, $Bi_4Ti_3O_{12}$ (BIT) belongs to a class of perovskite phase ferroelectric crystal with bismuth oxide-layered structure,[17,18] which have potential applications for optical memory, piezoelectric, and electro-optical device. According to the investigation made by Park *et al.*,[19] it is expected that substitution of a stable trivalent cation can improve the properties of BIT, while Nd-doped BIT has been receiving great attention for its larger remanent polarization than that of La-doped.[20] For Nd-doped BIT, many early studies were mainly concerned with ceramics, thin films, and particles,[21,22] but little has been regarding the $Bi_{4-x}Nd_xTi_3O_{12}$ (BNdT) nanotubes. The fabrication of 1D nanostructures of BNdT is of fundamental importance in investigating size-dependence physical properties, which have potential device applications, such as nanosensors, nanodectors, etc. In this paper, the BNdT nanotube arrays were fabricated by using a sol-gel method utilizing experimentally prepared AAO templates with pore diameters of 200 nm and 100 nm, respectively. Subsequently, the microstructure of the BNdT nanotube arrays was characterized in order to illuminate the mechanism of the transforming from nanoparticles to nanotubes. In addition, phonon scattering properties of BNdT nanotube arrays with different compositions were in-

[a)]Authors to whom correspondence should be addressed. Tel.: (86) 27 88665568. FAX: (86) 27 88662960. Electronic mail: guhsh583@yahoo.com.cn. (H. S. Gu). Tel.: (852) 27665680. FAX: (852) 23337629. Electronic mail: apywang@inet.polyu.edu.hk. (Y. Wang). Electronic mail: guanjg@whut.edu.cn. (J. G. Guan).

vestigated. Finally, the electric and ferroelectric properties of BNdT nanotube arrays with different compositions were investigated as well.

II. EXPERIMENTAL PROCEDURE

Two types of AAO templates with different pores diameter were fabricated by utilizing two-step anodization process as described previously.[14,23–25] For the preparation of BNdT precursor solutions, analytical grade bismuth nitrate $[Bi(NO_3)_3 \cdot 5H_2O]$ (99.0%), neodymium nitrate $[Nd(NO_3)_3 \cdot 6H_2O]$ (99.0%), and titanium butoxide $[Ti(OC_4H_9)_4]$ (98.0%) were used as starting materials. According to the stoichiometric composition reactants, the bismuth nitrate and neodymium nitrate were dissolved in 2-methoxyethanol, while titanium butoxide was stabilized by acetylacetone. A yellow, clear, and transparent BNdT precursor solution was obtained by mixing these two solutions together. The concentration of the final solution was adjusted to 0.1 M by adding 2-methoxyethanol. After the precursor solution was prepared, the AAO templates were immersed into the precursor solutions for 30 min and then removed. The AAO templates surfaces were carefully wiped using laboratory tissue. In order to obtain the perovskite phase, the templates containing the precursor were subsequently heated in air at 700 °C for 30 min by using a thermal annealing furnace. Finally, BNdT nanotube arrays were formed inside the pores of AAO templates.

The surface and cross-section morphologies of the BNdT nanotube arrays were characterized by field emission scanning electron microscopy (FESEM, HITACHI, S-4800) fitted with an energy dispersive x-ray spectrometry system (EDS) for element detection. The phase structure of the samples was carried out by an x-ray diffractometer (XRD) using Cu $K\alpha$ radiation ($\lambda = 0.15406$ nm) as the radiation source. The microstructures of the samples were performed using a transmission electron microscopy (TEM, JEM 2010). Before TEM testing, the AAO templates were dissolved by using 4 mol L^{-1} NaOH, and finally dispersed individual nanotubes were obtained. Raman scattering properties were characterized in backscattering geometry at room temperature by Renishaw RM-1000 confocal Raman microspectroscopy excited by 514.5 nm Ar^+ laser with power of 4.8 mW at the samples. To measure electrical and ferroelectric characteristic of as-prepared BNdT nanotubes arrays, both surfaces of the arrays were polished carefully with sand paper until BNdT nanotubes were emerged, and then a layer of Au with a thickness of 100 nm was sputtered on both sides of the arrays as conductive contacts. The measurement was performed at a nonlinear ferroelectric thin film testing system. The dielectric constant (ε_r) and dissipation factor ($\tan \delta$) were measured versus frequency using an impedance analyzer.

III. RESULTS AND DISCUSSION

Figure 1 shows the XRD patterns of as-prepared BNdT nanotubes with Nd content (x) of 0.85, 0.75, and 0.4 embedded in AAO templates with pores size of 200 nm. As can be seen that BNdT nanotube arrays are polycrystalline and part

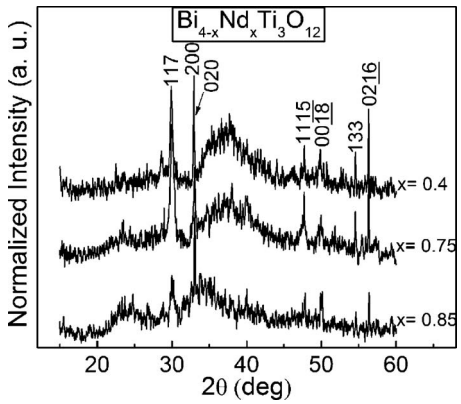

FIG. 1. XRD patterns of as-prepared nanotube arrays inside pores of AAO templates.

of diffraction peaks were appeared compare with that of ceramics. The diffraction peaks observed in XRD patterns matched well with an orthorhombic perovskite phase of BNdT (JCPDS No. 36–1486). The amorphous peaks (2θ) located at around 24° and 37° are attributed to the AAO templates, which begin to be crystallized only annealed at above 800 °C. One can also see that the intensities of plane (117) were suppressed with increasing the Nd ion substitute content in the compound. As well known that the (117) diffraction peak is the most intense for BNdT ceramics, while (200) diffraction peaks are the most for all samples, which indicate that the BNdT nanotube arrays are (200) orientated growth. Lattice parameters for BNdT nanotubes calculated from the XRD data and that for BIT are summarized in Table I. It's obvious that *c*-axis is decreased with increasing the contents of Nd ions in BIT matrix but the volume of lattices is increased dramatically when the doping level is high, which may be due to the lattice distortion caused by Nd ions with bigger atomic radius (2.64 Å) substitute for Bi with smaller atomic radius (1.63 Å).

The experimental processes are the same for preparation of BNdT nanotube arrays with different composition, hence BNdT (x=0.85) was provided here for morphologies observations. Figure 2 shows the field emission SEM images of BNdT (x=0.85) nanotube arrays. The as-prepared BNdT nanotubes were grown in AAO templates with pores size of 200 nm and 100 nm, respectively. One can see that the nanotubes are straight and roughly parallel to each other as shown in Figs. 2(b) and 2(d). The mean outer diameter of these nanotubes are about 200 nm and 100 nm, respectively, corresponding to the pores diameters of the AAO templates employed, which indicates that the diameters of nanotubes are confined by the AAO pores during their growth. In addition,

TABLE I. Lattice parameters data for BNdT nanotube arrays.

BNdT for different x	*a* (Å)	*b* (Å)	*c* (Å)	*V* (Å^3)
x=0	5.410	5.448	32.840	967.92
x=0.4	5.4304	5.4183	32.9434	969.31
x=0.75	5.4257	5.4196	32.7701	963.61
x=0.85	5.4263	5.5285	32.7629	982.86

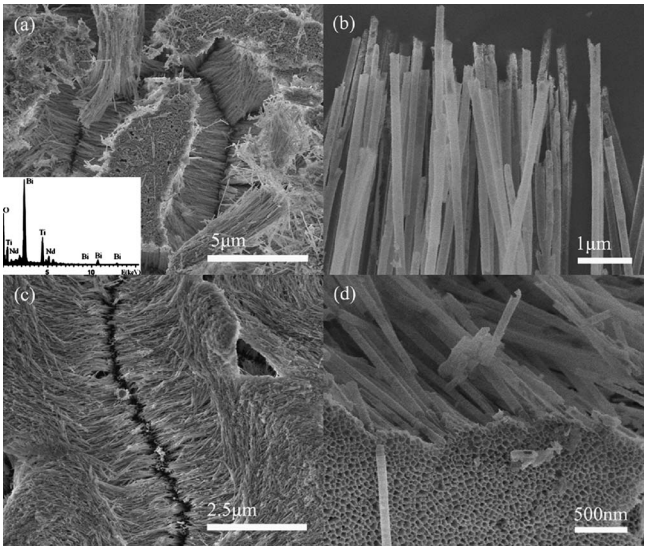

FIG. 2. Field emission SEM images of BNdT (x=0.85) nanotube arrays prepared in AAO templates with different pore diameters. (a) Nanotubes with outer diameters of 200 nm in low magnification (the inset is EDS spectrum), (b) nanotubes with outer diameters of 200 nm in high magnification, (c) nanotube with outer diameters of 100 nm in low magnification, and (d) nanotubes with outer diameters of 100 nm in high magnification.

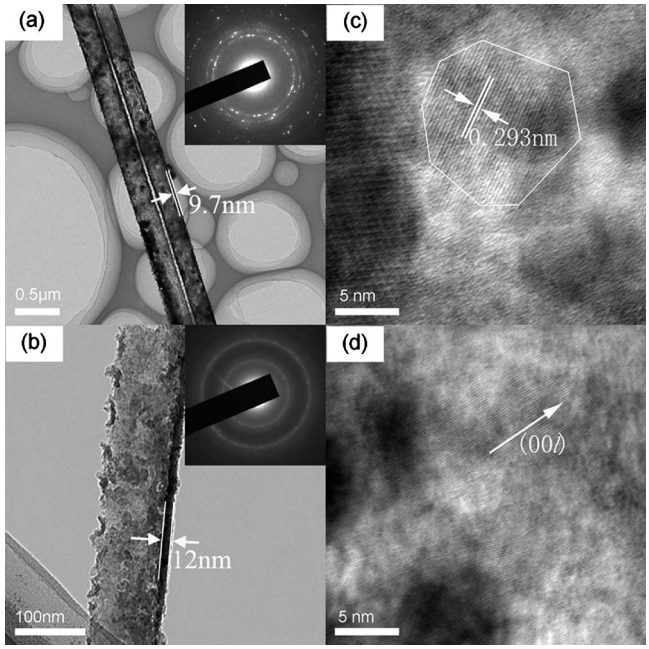

FIG. 3. TEM results of individual BNdT (x=0.85) nanotube with different outer diameters. (a) TEM image of BNdT nanotube with outer diameters of 200 nm (the inset is SAED pattern), (b) HRTEM image of BNdT nanotube with outer diameters of 200 nm, (c) TEM image of BNdT nanotube with outer diameters of 100 nm (the inset is SAED pattern), and (d) HRTEM image of BNdT nanotube with outer diameters of 100 nm.

the fractures resulted from samples preparation process clearly demonstrate that the nanotubes are hollow through the whole length, instead of just at the ends. The inset in Fig. 2(a) is EDS spectrum of BNdT nanotubes. It is clear that the nanotubes are consisted of Bi, Nd, Ti, and O element and the atomic ratio of these three elements Bi:Nd:Ti is about 3.19:0.88:3 confirmed by XPS technique. This demonstrates that the BNdT nanotubes have an ideal stoichiometric ratio.

TEM was employed to investigate the microstructures of BNdT (x=0.85) nanotubes. Figure 3 shows the typical TEM images of BNdT nanotubes after removed the AAO templates with pores diameter of 200 nm and 100 nm, respectively. It can be seen that the individual BNdT nanotubes are straight with the diameters of about 200 [Fig. 3(a)] and 100 nm [Fig. 3(b)], and with wall thickness of about 9.7 nm and 12 nm, respectively. The 200 nm diameter nanotubes have thinner tube wall than the 100 nm nanotubes, which was attributed to the larger tube wall area for the 200 nm diameter nanotubes as compared with the 100 nm nanotubes, while the same amount of precursor solutions were permeated into nanotubes under the same process conditions, such as precursor solutions concentration and immersion time. The insets in Fig. 3 are the selected area electron diffraction (SAED) patterns taken from each individual BNdT nanotube given in Figs. 3(a) and 3(b). The ringlike diffractions clearly demonstrate the polycrystalline features of BNdT nanotubes. Figures 3(c) and 3(d) are the high-resolution transmission electron microscopy (HRTEM) images of BNdT nanotubes with different diameter. It is found that the nanotubes are consisted of larger amount of small BNdT nanocrystallites with irregular morphologies and sizes of 10–20 nm. The interplanar distance of single nanoparticle is about 0.293 nm, corresponding to (117) planes as shown in Fig. 3(c). In addition, (00*l*) planes were appeared in Fig. 3(d). One can also see that nanotubes with diameters of 200 nm have better crystallites than the nanotubes with diameters of 100 nm, which can be confirmed from the definition of SAED and HRTEM results.

Figure 4 shows the Raman scattering spectra of BNdT (x=0.4, 0.75, and 0.85) nanotubes prepared in AAO templates with pores diameter of 200 nm. Raman selection rule allow 24 Raman active modes for orthorhombic BIT.[26] However, as shown in Fig. 4, the number of modes of all samples cannot fulfill the selection rule, which is partially due to possible symmetry breaking, distortion of TiO_6 octahedron induced from small size of BNdT nanotubes and low peak intensity as well as overlap of vibration modes. Compare with Raman data of BIT,[26,27] Nd substituted BIT exhibits intense phonon modes at about 130, 260, 433, 550, 760, and

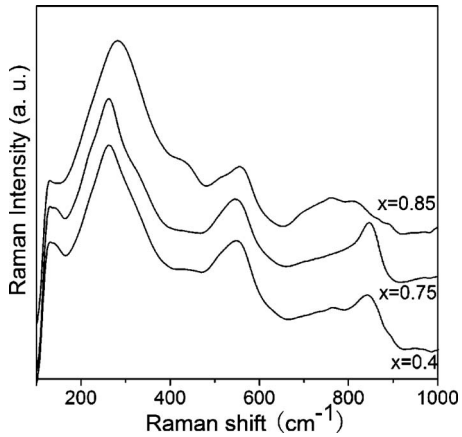

FIG. 4. Room temperature Raman spectra of BNdT (x=0.4, 0.75, and 0.85) nanotubes with different Nd substitution contents using AAO template with pore diameters of 200 nm.

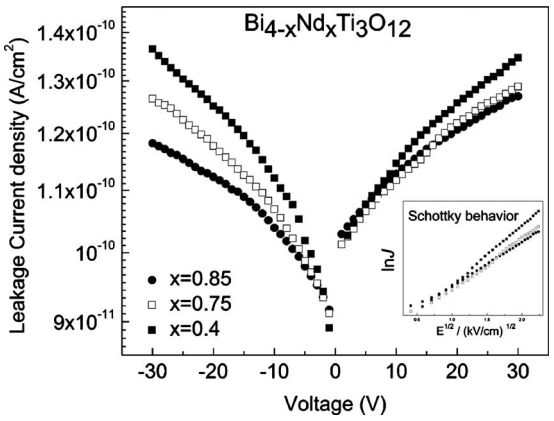

FIG. 5. Leakage current density in dependence of voltage for BNdT (x =0.4, 0.75, and 0.85) nanotube arrays inside AAO templates with pore diameters of 200 nm.

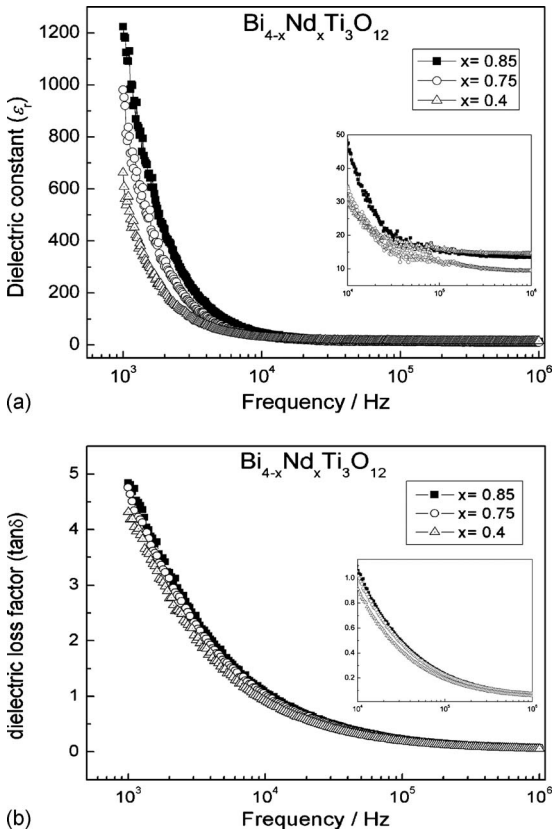

FIG. 6. Dielectric constant and dissipation factor in dependence of frequency for BNdT nanotube arrays(x=0.4, 0.75, and 0.85) at room temperature. The insets are curves of ε_r-f and tan δ-f in high frequency region from 10 kHz to 1 MHz, respectively.

850 cm^{-1} and many other weak features. The Raman phonon modes from 260 to 850 cm^{-1} are originated mainly from the vibrations of atoms inside the TiO_6 octahedral, which belong to the internal modes. The modes at 260 cm^{-1} are ascribed to the O–Ti–O bending vibration, and the 850 cm^{-1} mode is attributed to the symmetric Ti–O stretching vibration. As shown that the Raman peak at 130 cm^{-1} corresponding to the Bi atoms in the Bi_2O_2 layers weaken and broaden with increasing Nd content, which is the result of lattice distortion resulted from substitution of Bi atoms by Nd atoms. In addition, some obvious changes appeared at modes from 260 to 850 cm^{-1} with the increasing content of Nd in the compound, such as the shift of the mode at 260 to 280 cm^{-1}, softening and broadening of the modes at 550 cm^{-1}, disappearing of the mode at 850 cm^{-1} but discerning at 433 and 760 cm^{-1}. These changes for modes at high frequencies were induced by the increase in TiO_6 octahedron tilting and structural distortion with increasing the Nd content in the BIT lattice, which are consistent with the literature reported by Tomar *et al.*[28]

The insulating properties of BNdT (x=0.4, 0.75, and 0.85) nanotube arrays with different compositions were characterized by the *I-V* curves measured at room temperature. As shown in Fig. 5, the voltage changed from −30 to +30 V and the leakage current density were below 1.4×10^{-10} A/cm^2 for all three samples in which different Nd content doped. The insulating properties are better than that of $Bi_{3.15}Nd_{0.85}Ti_3O_{12}$ thin film and other rare-earth elements doped BIT thin films,[29–31] which is possibly caused by the discontinuous nanotubes or the bad contact between nanotubes and electrodes. One can also see that the leakage current density has a little decrease with the increasing content of Nd in the compound. The current density increases linearly with the external electric field in the region of high electric field strengths, suggesting an Ohmic conduction. At lower field the current density increases exponentially. As shown in the inset of Fig. 5, there are linear relationship between ln(J) and $E^{1/2}$ for three samples, which imply the conductivity results from Schottky emission mechanisms. The excellent insulating property is partly ascribed to the homogeneous distribution of BNdT grains, the improved crystallinity, and complete perovskite phase formation.

Figure 6 shows the dielectric constant and dissipation factor measured at room temperature as a function of frequency in the range from 1 kHz to 1 MHz. As shown in Fig. 6(a), the dielectric constants of three samples present intense drop in the range of frequency from 1 to 10 kHz. It is possible that this decrease in the dielectric constant in this frequency range is caused by space charge polarization or Maxwell–Wagner type interfacial polarization. With the increase in frequency the dielectric constants for all samples show very little dispersion. As can be seen from the inset of Fig. 6(a) the values of dielectric constants are in the range from 10–50 in the high frequency region from 10 kHz to 1 MHz. As shown in Fig. 6(b), the dielectric dissipation factors of three samples intensely decrease in the range from 4.8–0.05 with the increase in frequency from 1 kHz to 1 MHz, which indicate lower leakage current for three samples.

For investigating the ferroelectric feature of BNdT nanotubes, the polarization-electric (P-E) loop of BNdT (x=0.4, 0.75, and 0.85) nanotube arrays were recorded at 1 kHz with a Sawyer–Tower circuit and a digital oscilloscope. As a result, distinct ferroelectric hysteresis loops were obtained for the as-prepared samples. As shown in Fig. 7, the $Bi_{3.15}Nd_{0.85}Ti_3O_{12}$ nanotubes array has a larger polarization under high electric field compared with the other samples of BNdT with x=0.4 and 0.75, which exhibits well-saturated hysteresis loop with $2P_r$ and $2E_c$ values of about

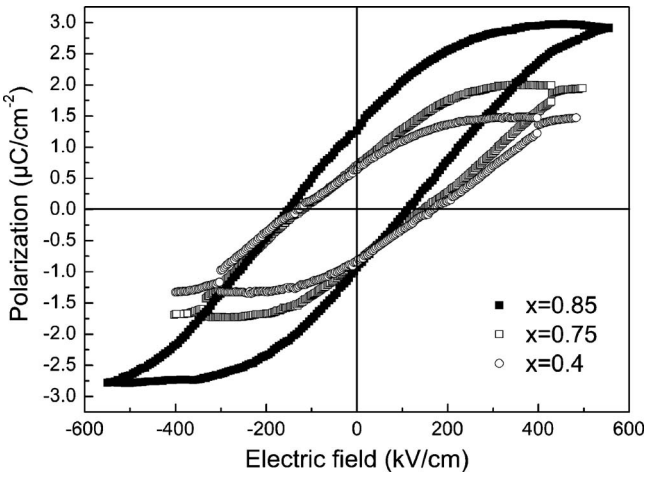

FIG. 7. P-E hysteresis loop for $Bi_{3.15}Nd_{0.85}Ti_3O_{12}$ nanotubes array inside AAO template with pore diameters of 200 nm.

2.2 $\mu C\ cm^{-2}$ and 260 $kV\ cm^{-1}$, respectively. According to the literature reported by Chon *et al.*,[32] P_r values of high *c*-axis orientated BNdT films are larger than that of non-*c*-axis orientated BNdT films. However the as-prepared sample in this paper with (200)-orientation has a larger remanent polarization. In other words, the spontaneous polarization vector of as-repared BNdT is closer to the *a*-axis rather than to the *c*-axis, which does not agree with the traditional theory and the research in respect to the cause is in progressing. In this experiment, the effective contact area of the ultrathin well nanotube arrays (10^9 nanotubes cm^{-2}) was calculated to be 6% with respect to that of a BNdT thin film. The normalized $2P_r$ was thus estimated to be 36.7 $\mu C\ cm^{-2}$, which was surprisingly similar to that of sol-gel prepared polycrystalline $Bi_{3.15}Nd_{0.85}Ti_3O_{12}$ films.[33]

IV. CONCLUSIONS

In summary, BNdT nanotube arrays were successfully fabricated by using a sol-gel template method utilizing AAO with pores diameters of about 200 nm and 100 nm, respectively. The as-prepared nanotube arrays possess polycrystalline phase and with orthorhombic perovskite structure. The obtained nanotubes have outer diameters of about 200 nm and 100 nm and wall thickness of about 9.7 nm and 12 nm, respectively. The internal modes from 260 to 850 cm^{-1} originated mainly from the vibrations of atoms inside the TiO_6 octahedral weaken and broaden with increasing Nd content, which indicates the increase in octahedron tilting and structural distortion. The change appeared at low frequency means Nd atoms partially substituted for Bi atoms at A-site. Furthermore, electric properties of BNdT (x=0.4, 0.75, and 0.85) nanotube arrays were measured. *I-V* curves of BNdT nanotube arrays show the leakage current density are 10^{-10} A/cm^2 magnitude, which is partly ascribed to the homogeneous distribution of BNdT grains and complete perovskite phase formation. The dielectric constants and dissipation factors present intense drop in the range of frequency from 1–10 kHz indicating polarization relaxation phenomenon. P-E loop of $Bi_{3.15}Nd_{0.85}Ti_3O_{12}$ nanotubes array shows $2P_r$ and $2E_c$ values are about 2.2 $\mu C\ cm^{-2}$ and 260 $kV\ cm^{-1}$, respectively, which clearly demonstrates the room temperature ferroelectricity. The studies for BNdT nanotube arrays with other content of Nd are in progress. The method employed here is favorite extended to fabricate nanotube and nanowire arrays of other complex oxides.

ACKNOWLEDGMENTS

The authors thank the National Science Foundation of China (NSFC) (Grant Nos. 90923013, 50872031, and 50902046), Research Fund for the Doctoral Program of Higher Education of China (Grant No. 20070512003), and the Natural Science Foundation of Hubei Province of China (Grant No. 2009CDB178).

[1] J. Scott, F. Morrison, M. Miyake, and P. Zubko, Ferroelectrics **336**, 237 (2006).
[2] Y. Luo, I. Szafraniak, and N. D. Zakharov, Appl. Phys. Lett. **83**, 440 (2003).
[3] B. I. Seo, U. A. Shaislamov, S.-W. Kim, H.-K. Kim, B. Yang, and S. K. Hong, Physica E **37**, 274 (2007).
[4] Y. Xia and P. Yang, Adv. Mater. **15**, 353 (2003).
[5] T. Tybell, C. H. Ahn, and J. M. Triscone, Appl. Phys. Lett. **75**, 856 (1999).
[6] D. D. Fong, G. B. Stephenson, S. K. Streiffer, J. A. Eastman, O. Auciello, P. H. Fuoss, and C. Thompson, Science **304**, 1650 (2004).
[7] J. F. Scott, J. Phys.: Condens. Matter **18**, R361 (2006).
[8] X. Y. Zhang, X. Zhao, C. W. Lai, J. Wang, X. G. Tang, and J. Y. Dai, Appl. Phys. Lett. **85**, 4190 (2004).
[9] J. J. Urban, W. S. Yun, Q. Gu, and H. Park, J. Am. Chem. Soc. **124**, 1186 (2002).
[10] G. Xu, Z. Ren, P. Du, W. Weng, G. Shen, and G. Han, Adv. Mater. **17**, 907 (2005).
[11] S. Karthäuser, E. Vasco, R. Dittmann, and R. Waser, Nanotechnology **15**, S122 (2004).
[12] X. Lu, D. Zhang, Q. Zhao, C. Wang, W. Zhang, and Y. Wei, Macromol. Rapid Commun. **27**, 76 (2006).
[13] H. S. Gu, Y. M. Hu, J. You, Z. L. Hu, Y. Yuan, and T. J. Zhang, J. Appl. Phys. **101**, 024319 (2007).
[14] A. P. Li, F. Müller, A. Birner, K. Nielsch, and U. Gösele, J. Appl. Phys. **84**, 6023 (1998).
[15] J. Kim, S. A. Yang, Y. C. Choi, J. K. Han, K. O. Jeong, Y. J. Yun, D. J. Kim, S. M. Yang, D. Yoon, H. Cheong, K. S. Chang, T. W. Noh, and S. D. Bu, Nano Lett. **8**, 1813 (2008).
[16] S. Singh and S. B. Krupanidhi, Phys. Lett. A **367**, 356 (2007).
[17] A. D. Rae, J. G. Thompson, R. L. Withers, and A. C. Willis, Acta Crystallogr., Sect. B: Struct. Sci. **46**, 474 (1990).
[18] E. C. Subbarao, Phys. Rev. **122**, 804 (1961).
[19] B. H. Park, B. S. Kang, S. D. Bu, T. W. Noh, J. Lee, and W. Jo, Nature (London) **401**, 682 (1999).
[20] T. Kojima, T. Sakai, T. Watanabe, H. Funakubo, K. Saito, and M. Osada, Appl. Phys. Lett. **80**, 2746 (2002).
[21] C. J. Lu, X. L. Liu, X. Q. Chen, C. J. Nie, G. L. Rhun, S. Senz, and D. Hesse, Appl. Phys. Lett. **89**, 062905 (2006).
[22] M. Liao, X. L. Zhong, J. B. Wang, H. L. Yan, J. P. He, Y. Qiao, and Y. C. Zhou, J. Cryst. Growth **304**, 69 (2007).
[23] H. Masuda and K. Fukuda, Science **268**, 1466 (1995).
[24] H. Masuda, F. Hasegawa, and S. Ono, J. Electrochem. Soc. **144**, L127 (1997).
[25] O. Jessensky, F. Müller, and U. Gösele, Appl. Phys. Lett. **72**, 1173 (1998).
[26] H. Idink, V. Sriknth, B. White, and E. C. Subbarao, J. Appl. Phys. **76**, 1819 (1994).
[27] P. R. Graves, G. Hua, S. Myhra, and J. G. Thompson, J. Solid State Chem. **114**, 112 (1995).
[28] M. S. Tomar, R. E. Melgarejo, and S. P. Singh, Microelectron. J. **36**, 574 (2005).
[29] C. H. Yang, Z. Wang, J. P. Zhai, G. P. Ma, X. Q. Sun, X. J. Yi, and J. R. Han, J. Cryst. Growth **264**, 312 (2004).

[30]C. H. Yang, Z. Wang, F. Y. Jiang, Y. L. Geng, B. Y. Zhu, X. J. Yi, G. P. Ma, and J. R. Han, J. Cryst. Growth **271**, 171 (2004).
[31]A. Z. Simòes, C. S. Riccardi, C. Quinelato, A. Ries, E. Longo, and J. A. Varela, Mater. Sci. Eng., B **113**, 207 (2004).
[32]U. Chon, H. M. Jang, M. G. Kim, and C. H. Chang, Phys. Rev. Lett. **89**, 087601 (2002).
[33]J. Yu, B. Yang, J. Li, X. M. Liu C. D. Zheng, Y. Y. Wu, D. Y. Guo, and D. M. Zhang, J. Phys. D **41**, 035304 (2008).